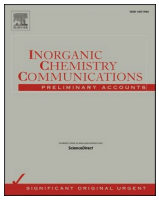
Inorganic Chemistry Communications 180 (2025) 114959



Contents lists available at ScienceDirect

Inorganic Chemistry Communications

journal homepage: www.elsevier.com/locate/inoche



Research Article



Synthesis and characterization of trimetallic AgPdAu alloy nanoparticles and their application in removal of methylene blue and methyl orange from wastewater

Sonalika Agarwal [a,b], Dong-Seog Kim [a], Lakshmana Reddy Nagappagari [a,c], Yeon-Tae Yu [a,*]

[a] Division of Advanced Materials Engineering, Research Center for Advanced Materials Development, Jeonbuk National University, Jeonju, Republic of Korea
[b] Graduate School of Advanced Science and Engineering, Hiroshima University, 1-3-1 Kagamiyama, Higashi, Hiroshima 739-8527, Japan
[c] Université de Caen Normandie, ENSICAEN, CNRS, LCS, Laboratoire Catalyse et Spectrochimie, 14000 Caen, France

ARTICLE INFO

Keywords:
Noble metals
Trimetallic alloy nanoparticles
Catalytic reduction
Organic dyes
Wastewater treatment

ABSTRACT

This study aimed to develop a novel AgPdAu trimetallic alloy nanoparticles (TANPs) with abundant catalytic sites for the efficient reduction of various dyes in wastewater and textile industries. The AgPdAu TANPs have shown excellent catalytic efficiency, as demonstrated via the reduction of Methylene blue (MB) and Methyl orange (MO) by $NaBH_4$. The entire conversion of MB to LMB is ultra-fast and took just 20 s when using 25 μL AgPdAu TANPs colloid with an apparent rate constant of 19.353 min^{-1}. In contrast, the catalytic decolorization of MO required 30 s when using 100 μL TANPs colloid with a rate constant of 6.794 min^{-1}. The results show that the AgPdAu TANPs have the best catalytic performance for reducing MB and MO compared to the bimetallic and monometallic nanoparticles (NPs) due to synergistic effects. Hence, AgPdAu TANPs are a potential candidate for reducing various dyes in real textile wastewater due to their outstanding catalytic activity and good stability.

1. Introduction

Water pollution is one of the most critical environmental challenges, presenting a grave peril to human well-being [1–3]. This not only threatens human health but also casts a long and menacing shadow over the delicate balance of aquatic ecosystems. Excessive discharge of wastewater laden with copious organic contaminants has spawned a significant and enduring threat to microorganisms, disrupting the equilibrium that sustains these vital ecosystems [4,5]. Even more concerning are certain aromatic pollutants, which are persistently present in the environment and notorious for their carcinogenic properties, casting a grim shadow over human health [6,7]. Among these culprits are azo dyes such as methylene blue (MB) and methyl orange (MO), which are frequently encountered in industrial wastewater, especially from textile manufacturing [8,9]. These dyes are notoriously hazardous to human health due to their toxicity and carcinogenicity, particularly when concentrated [3]. Therefore, the removal of these organic dyes from industrial wastewater has emerged as an important focus of interest in recent years, reflecting our common goal for a healthier and more sustainable future.

Numerous methods have been used to remove organic pollutants from industrial wastewater, including adsorption [10], membrane filtration [11], chemical oxidation [12], biodegradation [13], photocatalytic oxidation [14], catalytic reduction [15,16], etc. Developing effective, reusable, economic, and environmentally acceptable techniques to eliminate organic compounds from water is still challenging. Catalytic reduction of organic contaminants has garnered considerable attention due to its accessibility, ease of use, and high efficacy, particularly in light of the need to avoid the use of organic solvents, ensure safe operation, and conserve energy [17,18]. A major challenge for catalytic reduction to promote environmental friendliness is to use rational composition and structural design to build efficient catalysts that can boost the reduction effect of catalysts for organic pollutants such as MB and MO. It is widely recognized that without catalysts, the reduction of organic pollutants proceeds extremely slowly. Therefore, the development of catalysts for this reaction has been the focus of numerous investigations. It is generally known that the structure, shape, size, and chemical configuration of various nanomaterials have a significant impact on their catalytic activity. The desired catalytic activity of the materials can be achieved by continuously modifying these parameters. Exciting noble metal-based catalysts such as Au, Ag, Pd, and Pt nanoparticles are renowned for their exceptional physical, chemical,

* Corresponding author.
E-mail address: yeontae@jbnu.ac.kr (Y.-T. Yu).

https://doi.org/10.1016/j.inoche.2025.114959
Received 30 March 2025; Received in revised form 15 June 2025; Accepted 23 June 2025
Available online 27 June 2025
1387-7003/© 2025 Elsevier B.V. All rights are reserved, including those for text and data mining, AI training, and similar technologies.

and optical properties, making them versatile for a variety of applications, particularly in catalytic reduction [16,19]. Furthermore, the high surface-to-volume ratio of noble metal nanoparticles can significantly improve the interaction between reactants and catalysts [20]. Although the majority of monometallic particles exhibit excellent catalytic activity in comparison to their bulk metal counterparts, the catalytic performance of multi-metallic catalysts discovered in recent years is encouraging. In terms of their structure, size, and high volume-to-surface ratios, multi-metallic nanoparticles (NPs) have garnered more and more attention [21]. The novel physicochemical properties (e.g., electronic, optical, and magnetic), selectivity, and physical/chemical stability of trimetallic NPs produced by their monometallic and bimetallic counterparts, especially the interdependent nature of the catalytic structure, have recently attracted more scientific attention [2425]. The superior catalytic activity of trimetallic nanoparticles (TNPs) is due to pronounced synergistic effects arising from their unique composition and structural characteristics. Therefore, trimetallic NPs are also applied in several promising applications such as surface-enhanced Raman scattering, drug delivery, chemical sensing, plasmonics, catalysis, and semiconductors [22–26].

Although the interest in trimetallic nanoparticles (TNPs) has recently increased, only a few studies have been conducted on them to date. Sahoo et al. effectively prepared porous Au@Pd@Ru trimetallic nanoparticles for the reduction of several azo dyes and showed remarkable catalytic activity. [27]. Zhang et al. used a two-step electrodeposition technic for the successful synthesis of the hierarchical Cu-Ni-Pt dendrites. The results demonstrated that the trimetallic Cu-Ni-Pt dendrites presented excellent catalytic activities in reducing 4-nitrophenol (4-NP) to 4-aminophenol (4-AP) compared to bimetallic Cu—Ni dendrites. [28]. Li et al. produced trimetallic Au@PdPt nanoparticles for the process of oxygen reduction and showed excellent stability and catalytic activity [29]. Trimetallic Ni@Cu@Pd nanoparticles with blackberry structure were successfully prepared by Gong et al. [30] and demonstrated significant activity for the catalytic reduction of methylene blue (MB) and 4-nitrophenol (4-NP). There have been many reports on the improved catalytic performance of various types of multi-metallic nanoparticles [31–34]. These studies have suggested that trimetallic nanocatalysts can exhibit better catalytic activity in reducing organic pollutants than single and bi-metallic nanocatalysts by tuning their chemical composition and nanostructure [23,34].

In this study, well-ordered spherical-shaped novel AgPdAu trimetallic alloy nanoparticles (TANPs) were synthesized using a simple chemical method for the reduction of MB and MO. The catalytic activity of AgPdAu TANPs was investigated for the reduction of MB to LMB (leucomethylene blue) and MO to LMO (leucomethyl orange) in the presence of $NaBH_4$. These homogeneously synthesized AgPdAu TANPs showed superior catalytic activity in the catalytic reaction for reducing MB and MO compared to monometallic and bimetallic alloy nanoparticles. In addition, the rapid reaction rate of MB to LMB was achieved in just 20 s using a small quantity of TANPs. As far as we are aware, this is the initial research detailing the development of trimetallic AgPdAu alloy nanoparticles for the rapid catalytic reduction of organic dyes. This investigation is anticipated to provide an effective and straightforward approach for the simple production of trimetallic alloy nanoparticles that can serve as outstanding catalysts in catalytic reduction processes.

2. Experimental section

2.1. Chemicals

All chemicals were commercially sourced at analytical grade and used without additional purification. Hexadecyltrimethylammonium chloride (CTAC, $C_{19}H_{42}ClN$, 98 %), hexadecyltrimethylammonium bromide (CTAB, $C_{19}H_{42}BrN$, 99 %), silver nitrate ($AgNO_3$, 99.99 %), palladium chloride ($PdCl_2$, 99 %), sodium citrate ($C_6H_5Na_3O_7.2H_2O$, 98 %) was purchased from Showa Chemicals, and tetrachloroaurate trihydrate ($HAuCl_4{\cdot}3H_2O$, 99.99 %), methylene blue (MB) and methyl orange (MO) were provided by Sigma Aldrich. All experiments were conducted using deionized (DI) water.

2.2. Synthesis of AgPdAu trimetallic alloy nanoparticles (TANPs)

The AgPdAu TANPs were synthesized based on prior literature, with a few changes [35]. First, 80.0 mL of CTAB (15 mM) and 10.0 mL of CTAC (15 mM) deionized (DI) water solutions were combined in a 100 mL glass vessel. Then, 1 mL solutions of $AgNO_3$ (10 mM), H_2PdCl_4 (10 mM), and $HAuCl_4$ (10 mM) were gradually added to the aforementioned solution, and all were stirred at room temperature. Next, 570 μL of sodium citrate (100 mM) was added to the resulting solution. The glass vessel was then meticulously sealed and heated in an oven at 90 °C for 16 h before being allowed to cool naturally. The resulting mixture was centrifuged at 13,000 rpm for 30 min to separate the AgPdAu alloy nanoparticles. Afterward, distilled water was used to redisperse the collected AgPdAu TANPs for future use. The same process was used to prepare pure Ag, Pd, Au, and AgPd, AuPd, and AgAu nanoparticles by combining the Ag, Pd, and Au precursors (details are shown in Table S1).

2.3. Characterizations

The morphologies of the synthesized AgPdAu TANPs were observed using high-resolution transmission electron microscopy (TEM) (JEOL, JEM-2010) with 200 kV accelerating voltage. The materials were dropped onto a formvar/carbon supported copper grid and dried overnight at 60 °C. Their crystalline structures were measured using X-ray diffractometry (XRD) (D/Max 2005, Rigaku) with CuK_α radiation (λ = 1.54178 Å). X-ray photoelectron spectroscopy (XPS) (Thermo Fisher Scientific, Multilab 2000) was conducted with monochromated Al Kα X-ray photons ($h\nu$ = 1486.6 eV) sources to confirm the surface chemical states of the elements present in the prepared samples. The binding energies of the adventitious carbon (C 1 s) peak observed at around 285 eV were used for the calibration of other peaks. UV–vis. Spectra were measured using a spectrometer (Shimadzu, UV-2550) with 1 cm path length quartz cuvettes in the wavelength range of 200 to 800 nm at room temperature.

2.4. Catalytic activity of organic dyes

The catalytic activity of the AgPdAu TANPs was examined by reducing MB and MO, the two most frequently studied organic pollutants, using sodium borohydride ($NaBH_4$), which is a powerful reducing agent. Additionally, the catalytic activity of the monometallic and bimetallic nanoparticles was also evaluated for comparison. For the reduction of dyes MB and MO, a freshly prepared $NaBH_4$ aqueous solution (100 μL, 0.1 M) was added to the MB and MO aqueous solution (2.5 mL, 5 mM) in quartz cuvettes, respectively. Afterwards, 100 μl of each catalyst (Ag, Pd, Au, AgPd, AgAu, and PdAu) dispersion or 25 μL of AgPdAu TANPs dispersion was incorporated into the MB and MO aqueous solutions, and the color change was immediately observed using a UV–Vis spectrophotometer. In the presence of the reducing agent $NaBH_4$, the blue color of MB and the orange color of MO gradually disappeared. The reduction reaction was monitored as a function of time using UV–vis absorption spectroscopy.

The reaction kinetics to determine the effect of catalytic activity was used in the following equation [36,37]:

$$\ln(A_t/A_0) = ln(C_t/C_0) = -kt \quad (1)$$

where A_0 and A_t represent the peak absorbance at the starting stage and reaction time t, t is the reaction time, and k is the first-order rate constant (min^{-1}). The concentrations of organic dye at the start of the reaction and at time 't' are C_0 and C_t, respectively.

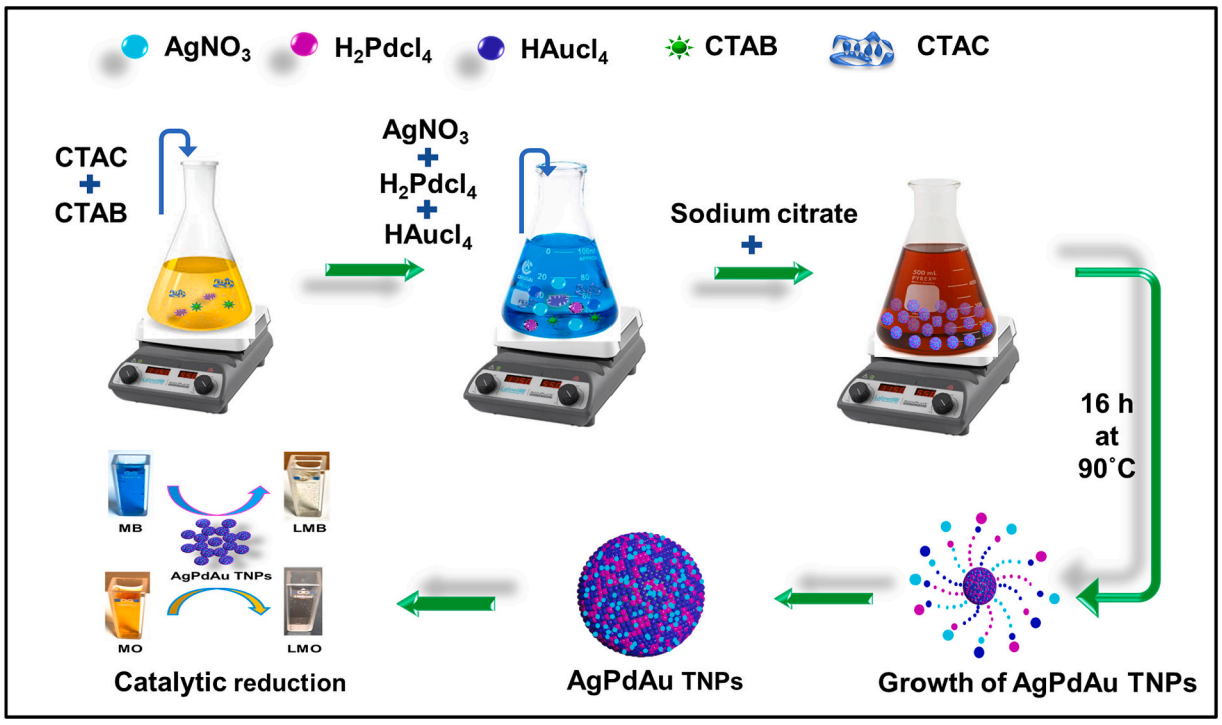


Fig. 1. The systematic illustration for the synthesis of AgPdAu TANPs.

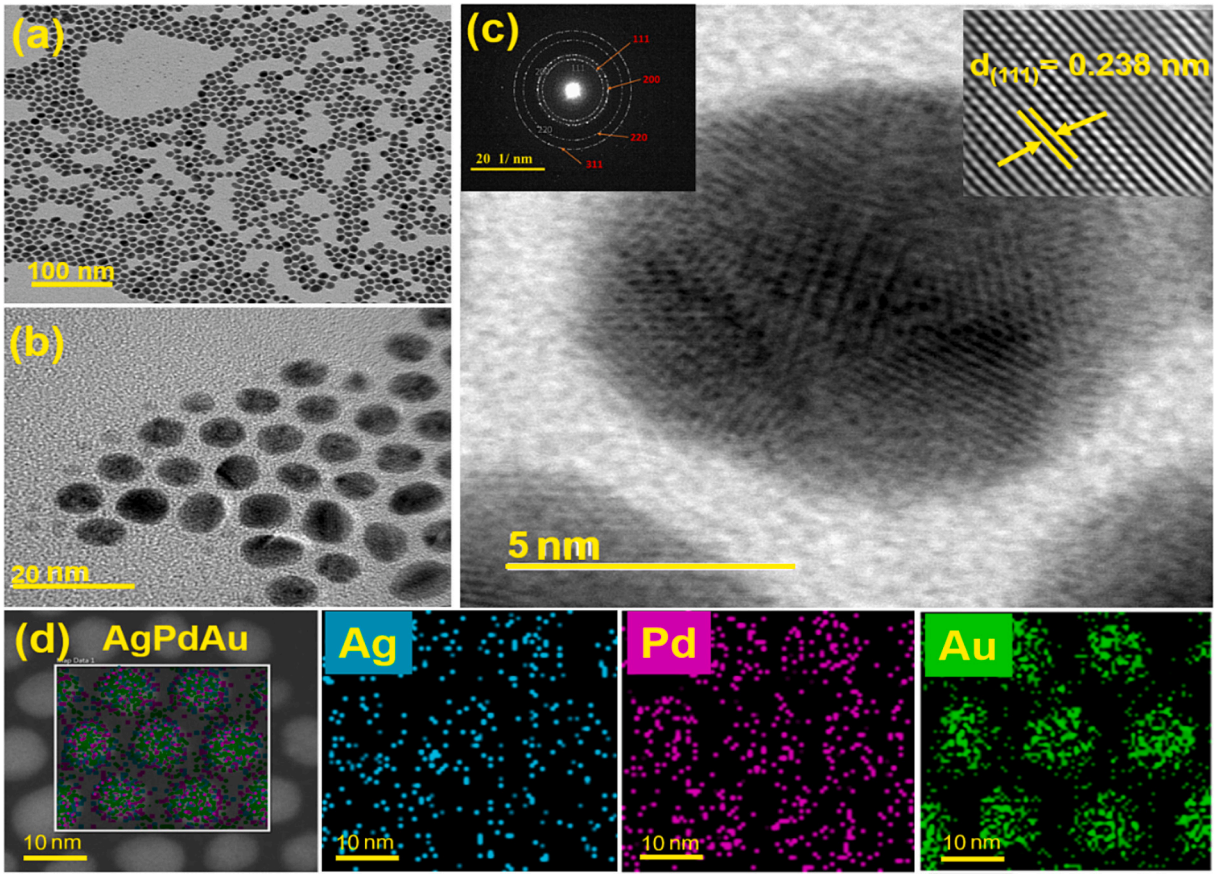


Fig. 2. TEM images (a-b) uniformly dispersible AgPdAu TANPs, (c) HR-TEM image of AgPdAu TANPs (Right side inset: interplanar distance and left side inset: Selected area diffraction pattern), (d) High-angle annular dark-field image of AgPdAu TANPs with EDS mapping of the Ag, Pd, and Au elements corresponding to the HAADF image.

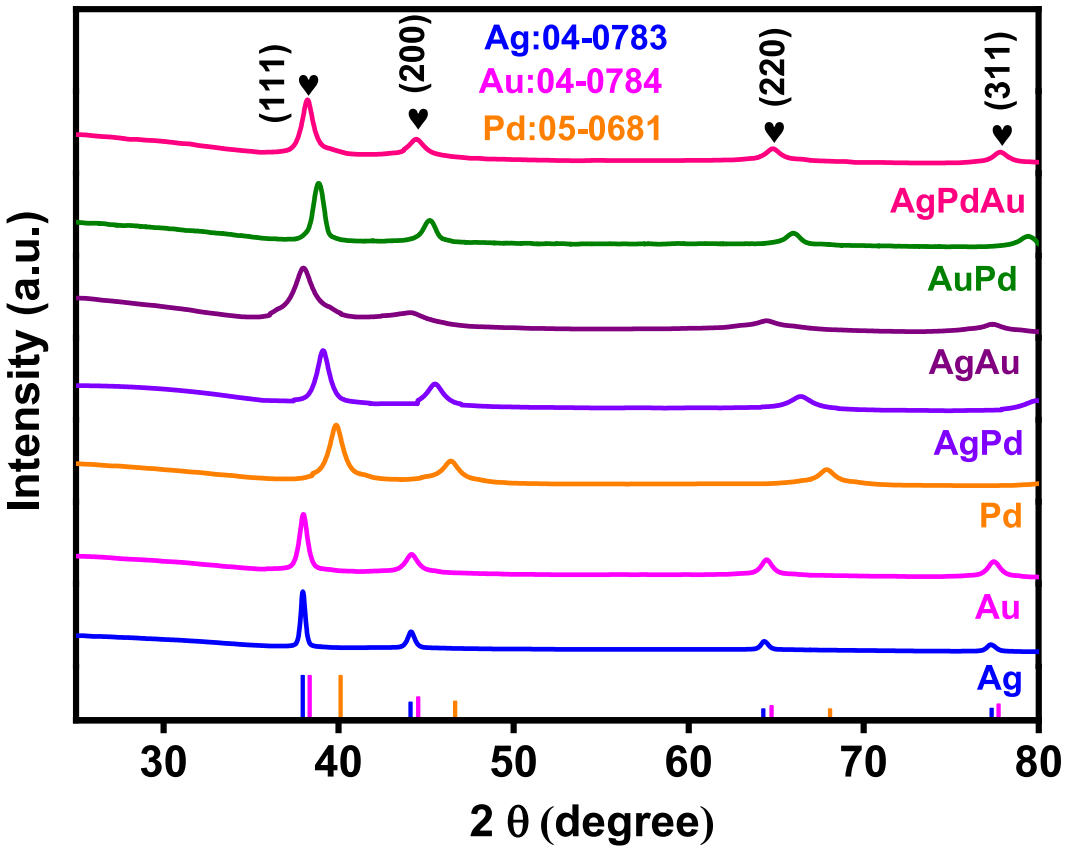


Fig. 3. XRD spectra of as-synthesized trimetallic AgPdAu, bimetallic (AgPd, AgAu & AuPd), and monometallic (Ag, Pd, and Au) NPs.

3. Results and discussion

3.1. Formation and structural characterization of AgPdAu TANPs

In this manuscript, we introduce for the first time a one-pot strategy to prepare trimetallic AgPdAu alloy nanoparticles through the chemical method of $AgNO_3$, H_2PdCl_4, and $HAuCl_4$, by using CTAB and CTAC surfactant and sodium citrate as reducing as well as stabilizing reagents (Fig. 1). Subsequently, the morphology and elemental composition of AgPdAu TANPs were systematically examined. The TEM images of as-prepared AgPdAu TANPs are displayed in Fig. 2a and b. The AgPdAu nanoparticles have an average particle size of 8 nm, with spherical in shape, and were evenly distributed. The HRTEM of AgPdAu TANPs (Fig. 2c) shows well-defined lattice fringes with an adjacent lattice spacing of 0.238 nm (marked in yellow, inset of Fig. 2c), which matches well with the (111) planar distance of AgPdAu, confirming the formation of Ag, Pd, and Au as a trimetallic alloy. The direction of the (111) facet differs in one particle, revealing the polycrystalline structure of AgPdAu alloy nanoparticles. This result is corroborated by the pattern of diffraction spots, which are superimposed on the rings in the SAED pattern, showing that each AgPdAu particle has a polycrystalline structure (Fig. 2c inset, left side). It is interesting to note that the SAED patterns of AgPdAu alloy NPs match with the XRD diffraction patterns seen in Fig. 3, which exhibit the (111), (200), (220), and (311) planes of Ag, Au, and Pd. In addition, high-angle annular dark-field scanning transmission electron microscopy (HAADF-STEM), with EDS elemental mapping, was performed to distinguish the distribution of the Ag, Pd, and Au elements (Fig. 2d). The resulting patterns demonstrated that Ag, Pd, and Au are allocated uniformly throughout the whole nanostructure of AgPdAu TANPs, which is further proof that the AgPdAu alloy formed. Hence, these results confirmed that the AgPdAu trimetallic alloy nanostructure was successfully synthesized. Furthermore, the typical TEM images of monometallic (Ag, Pd, Au) and bimetallic (AgAu, AgPd, and AuPd) nanoparticles were shown in Fig. S1 (a-g). From Fig. S1, it can be seen that all monometallic and bimetallic nanoparticles exhibit an almost spherical shape and smooth surface with uniform distribution. The average diameters of Ag, Pd, Au, AgAu, AgPd, and AuPd nanoparticles were around 42, 13, 20, 12, 21, and 15 nm, respectively. As a result, it is clear that the one-pot preparation method produced consistent multi-metallic (mono, bi, and tri) nanoparticles in high yield.

X-ray powder diffraction was used to investigate the crystallographic properties of the as-prepared nanoparticles. The XRD patterns of AgPdAu TANPs as well as monometallic (Ag, Pd, Au) and bimetallic (AgPd, AgAu, AuPd) are presented in Fig. 3. Here, AgPdAu TANPs exhibited four dominant diffraction peaks at 38.19°, 44.41°, 64.7° and 77.7° for the (111), (200), (220), and (311) planes, respectively with the face-centered cubic (FCC) structure, which are intermediate between those of pure Ag (JCPDS 04–0783, in blue), Pd (JCPDS 05–0681, orange) and Au (JCPDS 04–0784, pink). This shifting in peaks suggested that AgPdAu alloy nanoparticles had formed [38,39]. Additionally, it can be seen that the acquired XRD pattern of bimetallic AgAu nanoparticles is often comparable to that of individual Ag and Au. [40]. However, the interlayer distances between Ag and Au are too small for it is difficult to easily distinguish them due to limitations in the XRD technique [41]. The XRD pattern of the AgPd nanoparticles (Fig. 3) revealed that each diffraction peak is situated between the peaks of pure Ag and pure Pd, further indicating the formation of the AgPd alloy. Similarly, the shifting in four peaks for the (111), (200), (220), and (311) planes at the same 2θ values was observed for AuPd nanoparticles (shown in Fig. 3) as compared to their mono counterparts Au (JCPDS 04–0784) and Pd (JCPDS 05–0681). As a result, the shifts in the XRD peaks signify the formation of alloy nanoparticles. Selected area electron diffraction (SAED) technique was utilized to examine various areas of the trimetallic samples in order to further determine the distribution of Ag, Au,

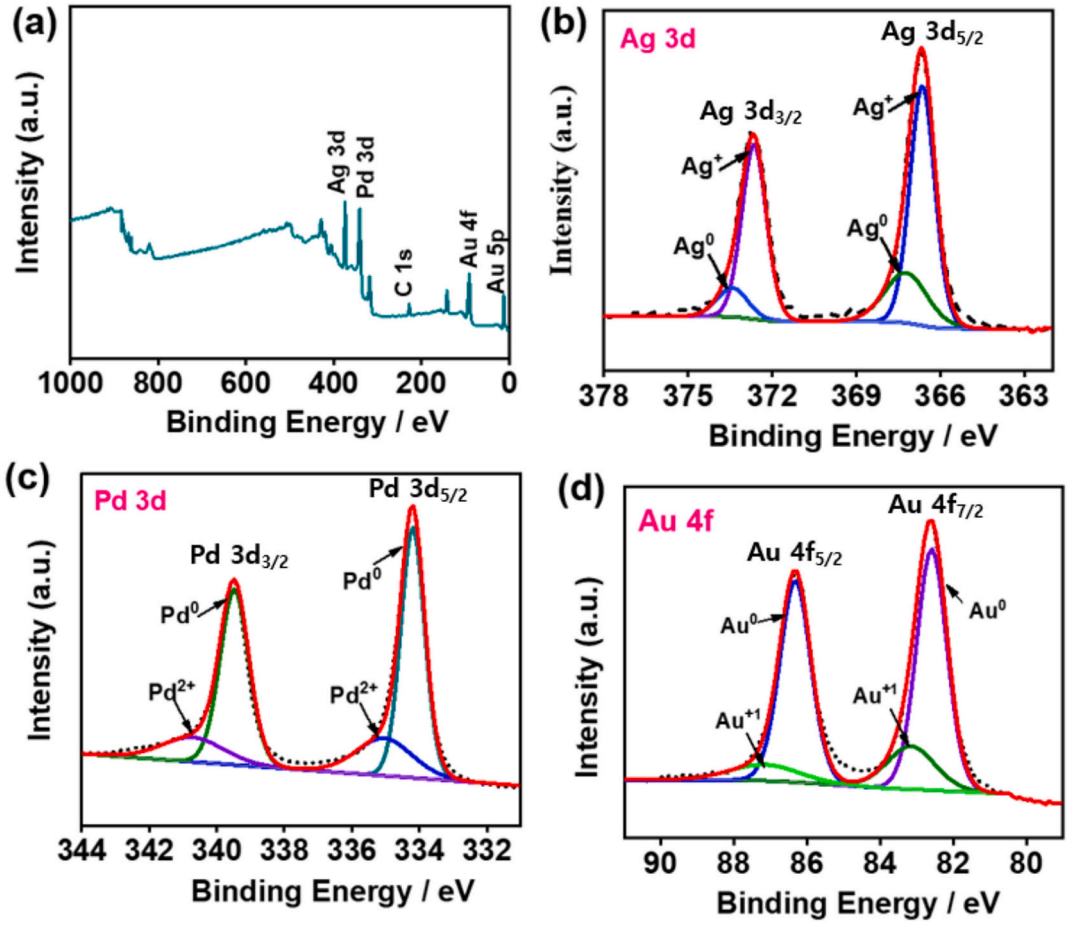


Fig. 4. XPS spectra of as-synthesized AgPdAu TANPs, (a) XPS survey scan, (b) Ag 3d, (c) Pd 3d, and (d) Au 4 f.

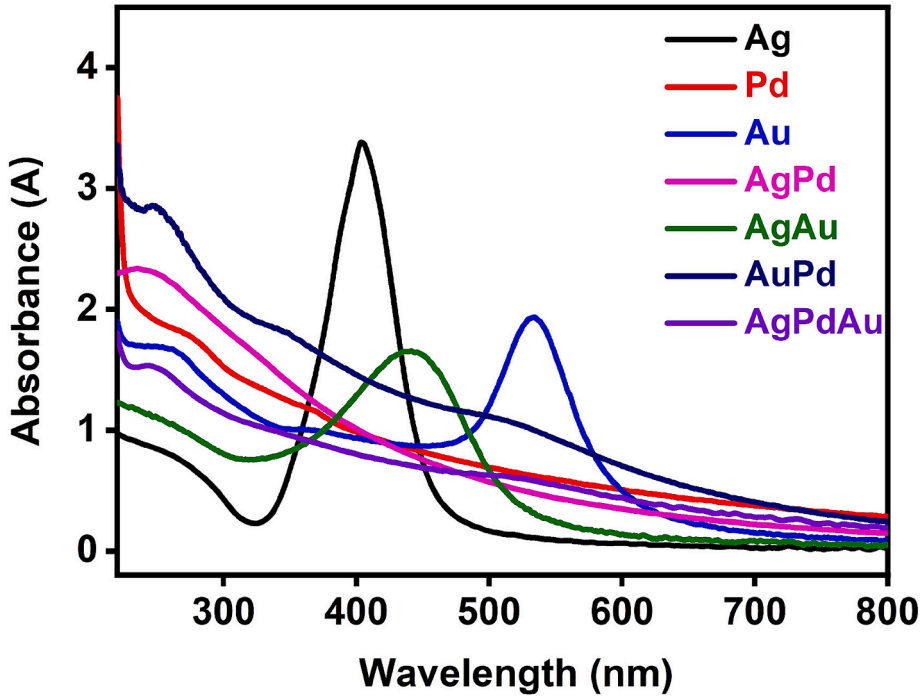


Fig. 5. UV–vis. Absorption spectra of as-synthesized trimetallic AgPdAu alloy NPs, bimetallic (AgPd, AgAu & AuPd) alloy NPs, and their counterparts in water.

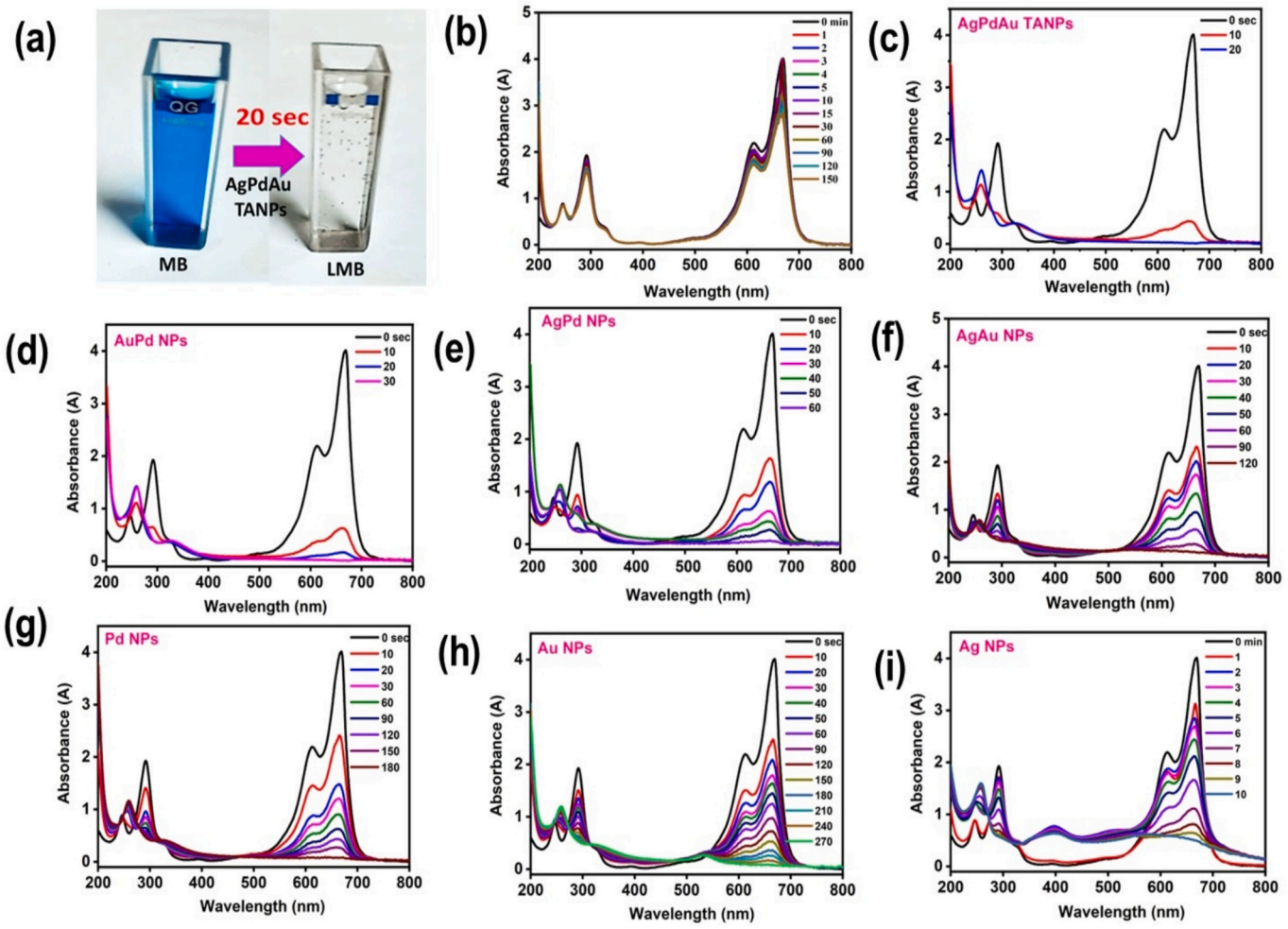


Fig. 6. (a) The change in color of MB to LMB after catalytic reduction by AgPdAu TANPs. The UV–vis. Spectra of MB (b) without catalyst, (c) AgPdAu TANPs, (d) AuPd NPs and (e) AgPd NPs (f) AgAu NPs, (g) Pd NPs, (h) Au NPs and (i) Ag NPs as catalysts, respectively.

and Pd inside the samples. The polycrystalline nature of all nanoparticles is often represented by the SAED patterns of AgPdAu (Fig. 2c, inset). Additionally, the XRD diffraction patterns are also consistent with the SAED patterns of the AgPdAu trimetallic nanoparticles (Fig. 3). The diffraction peak widths of trimetallic and bimetallic alloy NPs are much broader than those of monometallic NPs, as shown in Fig. 3. This means that the alloy NPs are composed of smaller crystalline particles as compared to monometallic NPs and undergo crystalline deformation, which creates many defects such as vacancies, dislocations, twins, and surface steps.

X-ray photoelectron spectroscopy (XPS) was used to acquire further proof of the chemical composition of AgPdAu TANPs (Fig. 4). The non-destructive, very sensitive analytical method known as XPS can provide important details about the chemical state and composition of the catalyst's surface. The typical XPS spectra of Ag 3d, Au 4 f, and Pd 3d obtained from the AgAuPd networks are displayed in (Fig. 4a). The electron binding energies of the Ag $3d_{5/2}$ and Ag $3d_{3/2}$ orbitals are shown in a high-resolution survey spectrum in (Fig. 4b). These energies can be further divided into the doublet peaks with binding energies of 366.68 eV and 372.88 eV that correspond to metallic silver (Ag^0) [42], and the peaks with binding energies of 367.23 eV and 373.41 eV that are assigned to Ag^+ can be recognized to the AgPdAu alloy of the formation [43,44]. These values of binding energy levels vary slightly and might be caused by alterations in the chemical environment. Palladium has XPS spectra at binding energies of 334.20 eV and 340.15 eV, which are ascribed to the Pd $3d_{5/2}$ and Pd $3d_{3/2}$, respectively (Fig. 4c). The coexistence of the two peaks indicates that metallic Pd^0 has formed [45]. A small percentage of species are showing signs of Pd alloy formation on the surface of nanoparticles. The typical XPS peaks of metallic Au are at 82.60 eV ($4f_{7/2}$) and 86.33 eV ($4f_{5/2}$)[49], and the Au 4 f peak is separated into four peaks in Fig. 4d. Two low binding energy peaks of the Au 4 $f_{7/2}$ components can be attributed to the Au^0 and Au^{+1} species, respectively, in the deconvoluted spectrum, which has two peaks at 82.55 and 83.21 eV [46]. The existence of Au^{+1} species is relatively very small as compared to Au^0 species. Due to charge transfer and electronic disturbances among them, the binding energies of silver (368.2 eV, $3d_{5/2}$), palladium (335.4 eV, $3d_{5/2}$), and gold (84.0 eV, $3d_{7/2}$) tend to move to lower values in trimetallic systems. From these XPS results, it is confirmed that Ag Ag-rich AgPdAu alloy was formed on the surface of AgPdAu TANPs.

The UV–vis. Spectra of the AgPdAu TANPs colloids as well as monometallic (Ag, Pd & Au) NPs and bimetallic (AgPd, AgAu and PdAu) alloy nanoparticles are presented in Fig. 5. The pure Ag NPs exhibit their characteristic absorption peak at 404 nm, and surface plasmon resonance (SPR) peak of Au nanoparticles shows at 533 nm, whereas the peak of the SPR band of analogous alloy AgAu appears between Ag and Au peaks around 441 nm (green line) [47,48]. The synthesized AgAu alloy NPs showed a single SPR peak, indicating that they were homogenous and uniformly alloyed [49]. Fig. 5 illustrates the absence of an absorption peak in the Pd colloidal solution in the range of 200–800 nm. But when Pd was added to the bimetallic colloidal samples, such as AgPd and AuPd, as well as to the AgPdAu trimetallic colloids solution, the SPR

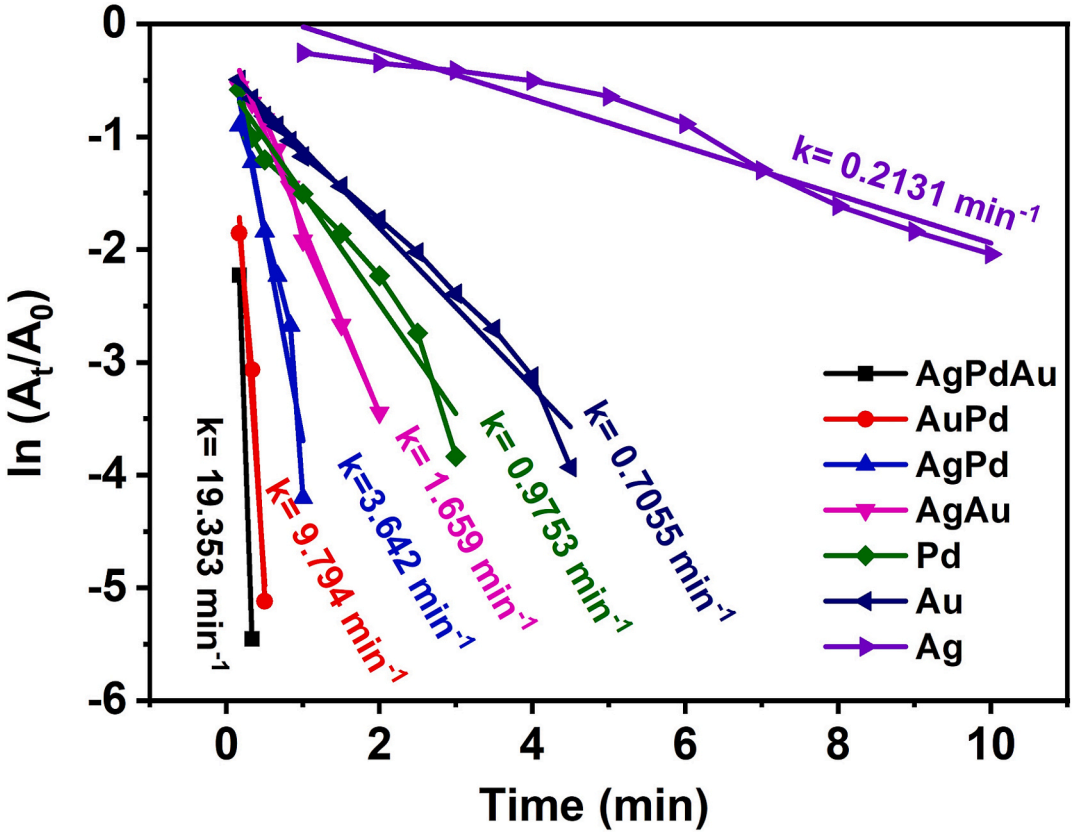


Fig. 7. Comparative plot of $\ln(A_t/A_0)$ against reaction time for the catalytic reduction of MB by different catalysts.

bands completely disappeared, which is consistent with earlier studies [50,51]. Consequently, the change in the absorbance characteristics of the AgPdAu TANPs compared to their individual metal counterparts confirms the formation of the AgPdAu alloy phases.

3.2. Catalytic reduction of methylene blue (MB)

In this section, the reduction of methylene blue (MB) through a comparison investigation of the catalytic activities of monometallic (Au, Ag, Pd), bimetallic (AgPd, AgAu, AuPd), and trimetallic (AgPdAu) nanoparticles has been carried out. The catalytic reduction capability of nanoparticles was investigated by reducing MB in the presence of $NaBH_4$. MB has blue color when it is in its oxidized state, but when it is reduced, it turns into the colorless chemical leucomethylene blue (LMB) (Fig. 6a). The UV–vis., absorption spectra of reduction of MB by $NaBH_4$ in the absence and presence of nanostructures are shown in Fig. 6 and exhibit a strong distinctive absorption peak at 669 nm, allocated to π -π^* transition and shows shoulder peak at 614 nm [6]. As can be seen from Fig. 6b, the catalytic reduction cannot occur without the catalyst, and the MB peak at 669 nm remained stable for 150 min. It is obvious that without a catalyst, the $NaBH_4$ cannot convert MB to LMB. As a result, the presence of a catalyst is crucial for the reduction of organic dyes. According to the results shown in Fig. 6(c-i), the characteristic MB peak intensity rapidly decreased, and the blue color solution of MB dye entirely vanished within a few seconds upon the addition of the synthesized catalysts, AgPdAu TANPs, as well as bimetallic alloy nanoparticles (BANPs) (AgPd, AgAu, AuPd) and monometallic nanoparticles (MNPs) (Ag, Pd, Au) alongside $NaBH_4$. In the process of catalytic reduction of dye, the catalyst can transport the electron from BH_4^- to surface-adsorbed MB, as a result, MB is reduced [52]. From Fig. 6c, it is also observed that when trimetallic AgPdAu nanoparticles were added to MB dye in the presence of $NaBH_4$, then the full reduction reaction of MB was completed within 20 s, which is very fast compared to literature reports. Interestingly, for the complete and fastest reduction of MB to take place for 25 μL (very little). The AgPdAu trimetallic nanoparticles colloid was used with $NaBH_4$, whereas 100 μL of bimetallic and monometallic nanoparticles colloids were used for the effective reduction of MB. The real-time practical application of the reduction of MB to LMB is also carried out and displayed in a video (see supporting information video). In this video, it can be noted that the blue color of MB changed to colorless in less than 20 s, which is a very fast reduction. These results reflected that multi-metallic nanostructure (AgPdAu) showed superior catalytic activity as compared to bimetallic and monometallic nanoparticles, for the reduction of MB.

According to Fig. 6 (e-i), when monometallic nanostructures were used, Pd NPs showed complete dye reduction in 3 min, Au NPs demonstrated 90–98 % dye reduction in 4.5 min, and Ag NPs demonstrated very sluggish reduction, taking 10 min to eliminate 70–80 % dye. For binary nanostructures, 90–98 % of dye was reduced in 30 s, 60 s, and 180 s for AuPd, AgPd, and AgAu BANPs, respectively. The catalysis by AuPd is much faster than the AgPd, AgAu catalysts, and revealed that the AuPd BANPs are an effective catalyst for the reduction process. Here, the surface plasmon resonance effect of Ag in the presence of Pd played a crucial role in the fast degradation of MO. These findings showed that Pd, rather than Au or Ag, had the highest catalytic activity, and Pd-Ag-based bimetallic nanostructures showed superior catalytic activity for the reduction of MB.

The pseudo-first-order kinetic model explains the reduction of MB in the presence of catalysts and the $NaBH_4$ system. The linear fitting of $\ln(A_t/A_0)$ and the reaction time 't' can be used to estimate the catalytic reduction rate (k_{aap}) constant shown in Fig. 7. The calculated k_{app} values for Ag, Au, Pd, AgAu, AgPd, AuPd, and AgPdAu were 0.2131 min^{-1}, 0.7055 min^{-1}, 0.9753 min^{-1}, 1.659 min^{-1}, 3.642 min^{-1}, 9.794 min^{-1}, and 19.353 min^{-1}, respectively. The maximum k_{app} value is found for AgPdAu, whereas the lowest is found for pure Ag. Hence, the AgPdAu TANPs are 90, 27, and 20 times more active than the individual Ag, Au,

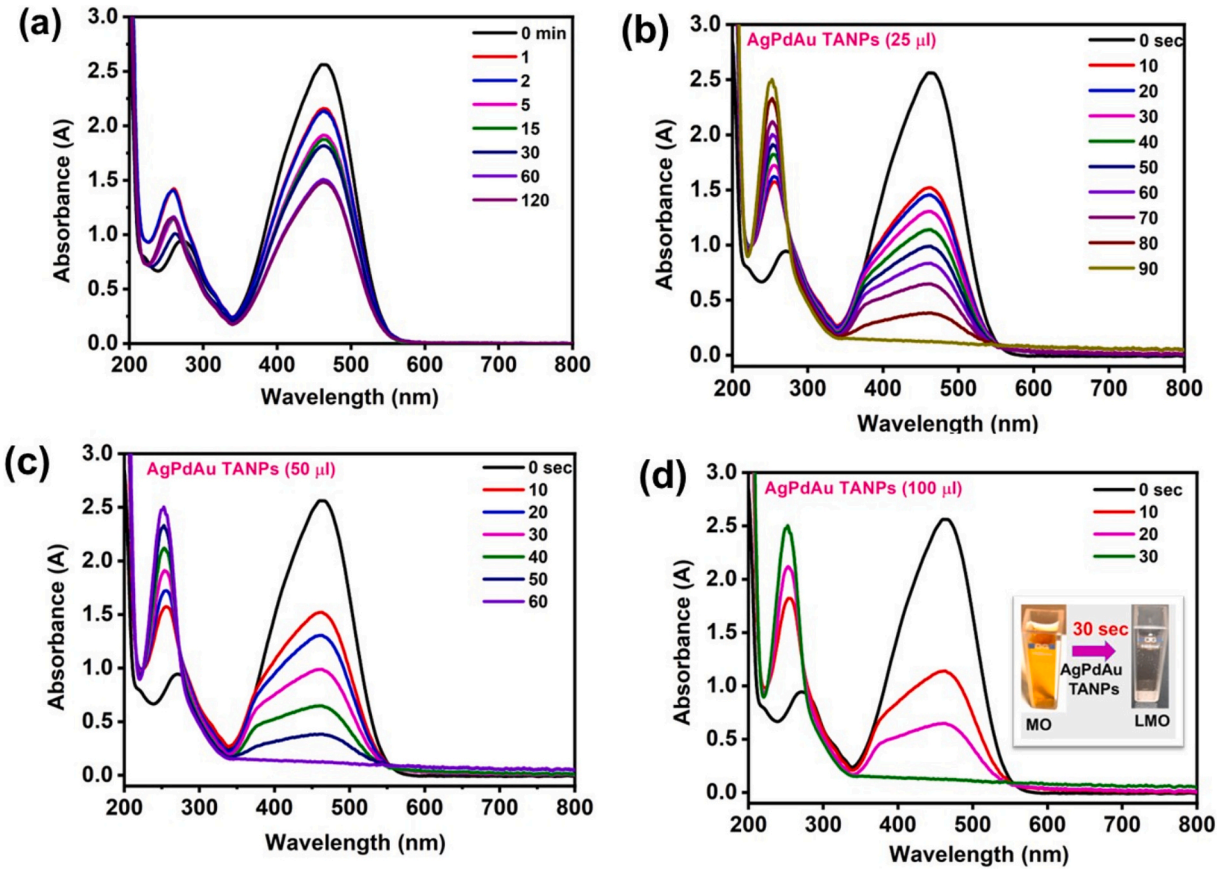


Fig. 8. UV–vis. Spectra of catalytic reduction of MO with $NaBH_4$ using (a) without catalyst, and with (b) 25 µl AgPdAu TANPs, (c) 50 µl AgPdAu TANPs (d) 100 µl AgPdAu TANPs, respectively (inset color change of MO to LMO).

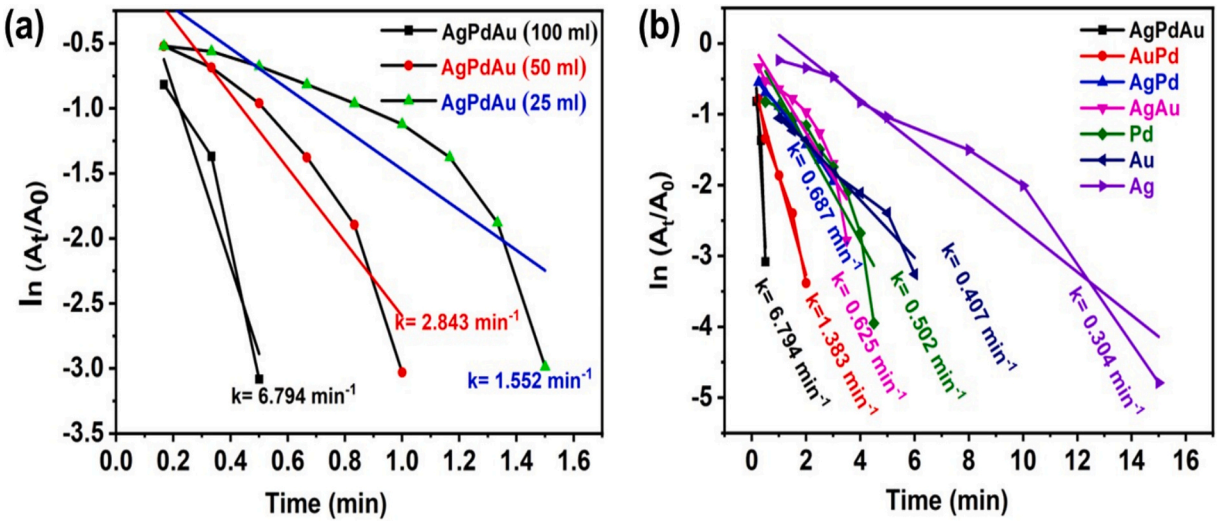


Fig. 9. Comparative plot of ln (A_t/A_0) versus reaction time for the catalytic reduction of MO (a) by different quantities of AgPdAu TANPs (b) by different catalysts (100 µL).

and Pd nanoparticles, respectively, whereas 12, 5, and 2 times more catalytically active than binary nanoparticles AgAu, AgPd, and AuPd, respectively. Overall, the AgPdAu trimetallic alloy nanostructure shows superior catalytic activity among all the other catalysts.

3.3. Catalytic reduction of methyl orange (MO)

Additionally, we performed borohydride reduction of another dye, methyl orange (MO), to see if the alloy NPs may be utilized as a catalyst for other dye reduction. When the UV–vis. Spectra of the MO solution were obtained, the characteristic wavelength (λ_{max}) appeared at 464 nm (Fig. 8a). Initially, $NaBH_4$ was introduced to MO and its UV–vis.

Table 1
Comparison of the catalytic activity of trimetallic alloy nanoparticles for the reduction of organic dyes.

S. No.	Catalyst	Dye	Amount of NPs	Reaction Time	Reaction rate constant K (min^{-1})	Ref.
1	PdPtCo TNPs	MB	1 mg	150 min	0.0116	[56]
2	Cu-Co-Ni TNPs	MB	30 mg	100 min	0.02588	[57]
3	Cu-Au-Ag nanobowls	4-NP	–	7 min	0.432	[58]
4	FeAgPt alloy	RHB	0.2 mg	15 min	0.256	[22]
5	PtPdBi NWs	PNP	15 μg	14 min	0.258	[59]
6	Au-Ag BNPs	MO	50 μl	3 min	0.5547	[53]
7	Au@Pd@Ru TNPs	PNP	100 μl	8 min	0.242	[27]
8	Ni@Cu@Pd TNPs	MB	0.5 ml	60 s	3.29	[30]
9	AgPdAu TANPs	MO	100 μl	30 s	6.794	This work
10	AgPdAu TANPs	MB	25 μl	20 s	19.353	This work

Spectrum was observed for 120 min. The MO wavelength absorption intensity in this process was reduced during the period of two hours relatively slowly, by barely 40 %. (Fig. 8a). After that, in the solution of azo dye (MO), the AgPdAu TANPs catalyst was introduced with $NaBH_4$. When the catalyst is introduced, the azo dye color changes from orange (N═N chromophore connected by two aromatic molecular systems) to colorless chemical leucomethylene orange (LMO) (−NH−NH) [53,54] as depicted in the inset Fig. 8d. The molecule of MO was initially adsorbed on the surface of AgPdAu TNP when the catalyst was added. It then acts as a catalyst, breaking the double bond N═N, potentially producing compounds with a single phenyl ring and amine groups, and decolorizing the MO [55]. Moreover, The UV–vis. Spectra were used to monitor the MO reduction process reaction with the addition of AgPdAu TANPs as a catalyst with $NaBH_4$, as shown in Fig. 8(b-d). The transformation of MO to hydrazine derivatives was ensured by the decreasing trend in intensity of the MO peak at 464 nm and the formation of a new intensity peak at 260 nm at the same time[51]. Here, for MO reduction, 25, 50, and 100 μL of AgPdAu TANPs colloids were added with $NaBH_4$, and these amounts took 90, 60, and 30 s, respectively, to complete the reduction (Fig. 8b to Fig. 8d). Furthermore, the calculated rate constants for 25, 50, and 100 μL of AgPdAu TANPs colloids, respectively, were 1.552, 2.843, and 6.794 min^{-1} (Fig. 9a). The overall results demonstrate that the reaction rate constant increases with increasing catalyst amount. This is because as the amount of NPs increases, the surface area of the active site of the nanocatalyst increases [53].

Additionally, the catalytic activities of monometallic (Ag, Au, and Pd) and bimetallic (AgPd, AgAu, and AuPd) nanoparticles towards the reduction of MO by $NaBH_4$ were investigated and are displayed in Fig. S2. The results indicate that in this case also pure Ag NPs exhibited the lowest catalytic activity (almost taking 15 min to complete reduction) compared to other monometallic Au (6 min) and Pd NPs (4.5 min), and also compared to bimetallic nanoparticles AgAu (3.5 min), AgPd (3 min), and AuPd (2 min). We also estimated the pseudo-first-order kinetics reaction rate and the estimated rate constants, which are depicted in Fig. 9 b, based on the reaction. The k_{app} values directly calculated from the slope of the straight line were 0.304 min^{-1}, 0.407 min^{-1}, 0.502 min^{-1}, 0.625 min^{-1}, 0.687 min^{-1}, 1.383 $min^{-1,}$ and 6.794 min^{-1} for Ag, Au, Pd, AgAu, AgPd, AuPd, and AgPdAu, respectively. Thus, the trimetallic AgPdAu nanoparticles are 22, 17, and 14 times more active than the individual constituents Ag, Au, and Pd, respectively. This result recommended that the synergistic effect of trimetallic AgPdAu nanoparticles improve catalytic reactivity due to the modulation of electronic structure.

For a clear illustration, we compared the catalytic activity of AgPdAu alloy trimetallic nanoparticles with some previously reported results for the reduction of organic dyes, which are provided in Table 1. As can be seen, the AgPdAu catalyst for MB and MO dyes exhibits the fastest reduction and highest activity when compared to other catalysts. The improved activity of the AgPdAu TANPs catalyst may be due to the synergetic effect of the Ag, Au, and Pd-containing nanoparticles.

3.4. Mechanism for catalytic reduction of organic dyes

The catalytic reduction of organic dyes, such as methylene blue (MB) and methyl orange (MO), through the use of AgPdAu TANPs in the

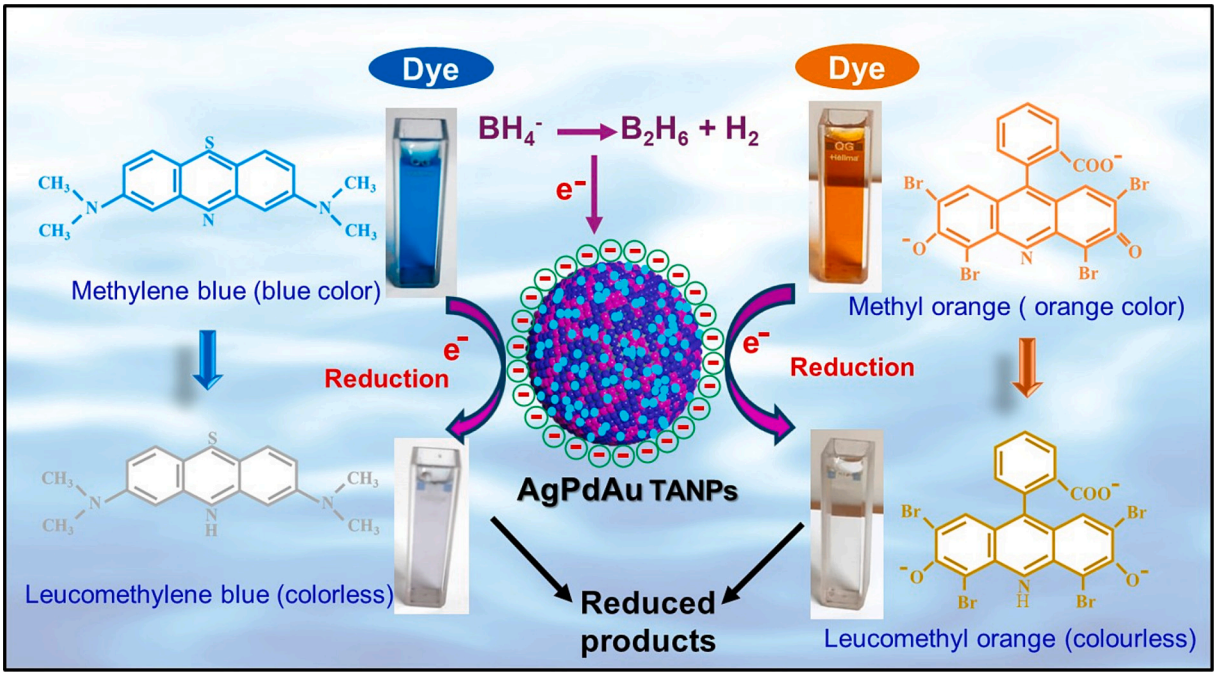


Fig. 10. Proposed mechanism of catalytic reduction of organic dyes with AgPdAu TANPs catalyst and $NaBH_4$.

presence of $NaBH_4$ involves a sophisticated mechanism that orchestrates electron transfer processes and exploits the unique properties of the catalyst. Crucially, the efficiency of this catalytic process hinges on the catalyst's ability to facilitate electron transfer between these species, in which AgPdAu TANPs play a pivotal role.

One of the basic principles of this mechanism is that the catalyst must possess an intermediate redox potential. This intermediate potential allows for the feasible transfer of electrons between the electron donor ($NaBH_4$) BH_4^- and the electron acceptors (MB and MO) [60]. Herein lies the magic of the trimetallic nanoparticles. In the MB/MO reduction mechanism, metal nanoparticles can catalyse the reaction by transferring active hydrogen species (H^+) to their surface to create metal hydride complexes. After reduction, the methylene blue (MB) and methyl orange (MO) spontaneously desorbed from the surface of the AgPdAu TANPs catalyst and diffused into the solution due to the weaker electrostatic action between the AgPdAu TANPs catalyst and LMB aqueous solutions changed into leucomethylene blue (LMB) and leucomethyl orange (LMO), as shown in Fig. 10.

The synergistic electron transfer and adsorption properties of trimetallic AgPdAu alloy nanoparticles (TANPs) greatly improved the catalytic reduction of organic dyes such as MB and MO. [47]. By functioning as an effective electron relay system, AgPdAu TANPs accelerate the rate of reaction by transferring electrons from the donor (BH_4^- ions) to the acceptor dye molecules through the catalytic surface. [61]. In this process, a negatively charged layer is formed surrounding the nanoparticles because of the BH_4^- ions donating electrons to the TANPs catalyst. By facilitating the flow of electrons from the catalyst to the dye molecules, this electron-rich surface promotes the reduction of the dye molecules to their corresponding leuco forms (LMB and LMO). AgPdAu TANPs' high surface area and variable surface chemistry improve dye adsorption through electrostatic interactions, π-π stacking, and van der Waals forces. This concentrates dyes at the catalyst surface and increases effective electron transfer. [47,62].

Additionally, the strong synergistic effects of trimetallic composition of AgPdAu alloy nanoparticles confer enhanced catalytic performance over their monometallic and bimetallic counterparts [48,63]. The combination of three different metals (Ag, Pd, and Au) optimizes electron density, improves charge transfer efficiency, and stabilizes reactive intermediates. This multi-metal interaction enhances organic dye adsorption capability and catalytic activity, allowing for effective MB and MO degradation [64]. The alloy's adjustable composition and numerous active sites increase redox characteristics and allow for faster reduction processes. As a result, the combined effects of adsorption, efficient electron relay, and synergistic interaction among the metallic components extensively improve AgPdAu TANPs' catalytic efficiency, making them highly effective for organic dye degradation [47,63].

Furthermore, the ultra-small size and alloy nanostructure of AgPdAu TANPs are not to be underestimated. This feature furnishes the catalyst with a significant quantity of active surface area, which is an important asset for improving catalytic activity. [65]. Specifically, the trimetallic alloy nanoparticles develop numerous crystalline defects, such as steps, which arise from internal crystalline deformation, on their surfaces during the alloying process. These defects are beneficial for generating a negatively charged layer on the surface of TANPs and can serve as significant active sites in catalytic reactions [63]. According to the results, Fig. 10 illustrates the essential mechanistic pathways involved in the catalytic reduction of dyes facilitated by the AgPdAu TANPs/NaBH4 system.This complex interaction between electrons and molecules is an elegant example of catalysis in the context of nanomaterials.

4. Conclusions

Here, we have reported a simple, straightforward synthesis approach for unique trimetallic AgPdAu alloy nanoparticles by using a chemical synthesis method. The TEM images of the AgPdAu TANPs confirmed their spherical shape. Such trimetallic AgPdAu alloy nanostructures for the reduction of MB and MO have not yet been investigated. The formation of AgPdAu alloy nanoparticle with Ag rich surface has also been demonstrated using XRD and XPS analysis techniques. All trimetallic AgPdAu nanoparticles were found to have a weak UV–vis. Absorption peak. In this study, it was found that the AgPdAu TANPs synthesized with $NaBH_4$ were excellent for catalytic reduction of MB and MO dyes. The AgPdAu noble TANPs, which are 20, 27, and 90 folds more active than the constituent metals Pd, Au and Ag, respectively, also showed the fastest reduction of MB to LMB within 20 s and the highest reaction rate k_{aap} value 19.353 min^{-1}. On the other hand, the catalytic decolorization of MO took 30 s with a reaction rate constant of 6.794 min^{-1} by using AgPdAu TANPs colloid nanoparticles. The remarkable catalytic performance of AgPdAu TANPs can be attributed to the crystal deformation that occurs during the alloying of the nanoparticles, which is more pronounced in the ternary alloy compared to the binary alloy.The synergistic alloying effects between Ag, Au and Pd nanoparticles resulted in the outstanding catalytic activity of AgPdAu catalysts compared to the monocular and binary catalysts. The high catalytic activity, quick reduction rate and simple synthesis approach suggest that AgPdAu TANPs are promising catalysts. This will be particularly useful in the treatment of colorful wastewater produced by the textile and dye production sectors.

CRediT authorship contribution statement

Sonalika Agarwal: Writing – original draft, Methodology, Investigation, Formal analysis, Data curation, Conceptualization. **Dong-Seog Kim:** Software, Formal analysis. **Lakshmana Reddy Nagappagari:** Writing – review & editing. **Yeon-Tae Yu:** Writing – review & editing, Visualization, Supervision, Resources, Project administration, Funding acquisition.

Declaration of competing interest

The authors declare that they have no known competing financial interests or personal relationships that could have appeared to influence the work reported in this paper.

Acknowledgements

This work was supported by 1) the BK21-FOUR program of the Ministry of Education and Human-Resource Development, South of Korea; and 2) the National Research Foundation of Korea (NRF) and the Commercialization Promotion Agency for R&D Outcomes(COMPA) grant funded by the Korea government (Ministry of Science and ICT) (RS-2025-02314407). 3) The Regional Innovation System & Education (RISE) initiative, funded by the Ministry of Education and administered by the National Research Foundation of Korea (NRF).

Appendix A. Supplementary data

Supplementary data to this article can be found online at https://doi.org/10.1016/j.inoche.2025.114959.

Data availability

Data will be made available on request.

References

[1] M. Thomas, G.A. Naikoo, M.U.D. Sheikh, M. Bano, F. Khan, Effective photocatalytic degradation of Congo red dye using alginate/carboxymethyl cellulose/TiO2 nanocomposite hydrogel under direct sunlight irradiation, J. Photochem. Photobiol. A Chem. 327 (2016) 33–43, https://doi.org/10.1016/j.jphotochem.2016.05.005.

[2] R. Das, V.S. Sypu, H.K. Paumo, M. Bhaumik, V. Maharaj, A. Maity, Silver decorated magnetic nanocomposite (Fe3O4@PPy-MAA/ag) as highly active catalyst towards

reduction of 4-nitrophenol and toxic organic dyes, Appl. Catal. B Environ. 244 (2019) 546–558, https://doi.org/10.1016/j.apcatb.2018.11.073.
[3] M.A. Ahsan, V. Jabbari, A.A. El-Gendy, M.L. Curry, J.C. Noveron, Ultrafast catalytic reduction of environmental pollutants in water via MOF-derived magnetic Ni and cu nanoparticles encapsulated in porous carbon, Appl. Surf. Sci. 497 (2019) 143608, https://doi.org/10.1016/j.apsusc.2019.143608.
[4] J. Lu, J. Fang, J. Li, C. Wang, Z. He, L. Zhu, Z. Xu, H. Zeng, Polydopamine nanotubes decorated with ag Nanoparticles as catalyst for the reduction of methylene blue, ACS Appl. Nano Mater. 3 (2020) 156–164, https://doi.org/10.1021/acsanm.9b01861.
[5] X. Liang, S. Zhu, Y. Zhong, J. Zhu, P. Yuan, H. He, J. Zhang, The remarkable effect of vanadium doping on the adsorption and catalytic activity of magnetite in the decolorization of methylene blue, Appl. Catal. B Environ. 97 (2010) 151–159, https://doi.org/10.1016/j.apcatb.2010.03.035.
[6] A.K. Abay, X. Chen, D.H. Kuo, Highly efficient noble metal free copper nickel oxysulfide nanoparticles for catalytic reduction of 4-nitrophenol, methyl blue, and rhodamine-B organic pollutants, New J. Chem. 41 (2017) 5628–5638, https://doi.org/10.1039/c7nj00676d.
[7] F. Subhan, S. Aslam, Z. Yan, M. Yaseen, K.A. Khan, Palladium nanoparticles decorated on ZSM-5 derived micro-mesostructures (MMZ) for nitrophenol reduction and MB degradation in water, J. Environ. Chem. Eng. 9 (2021) 105002, https://doi.org/10.1016/j.jece.2020.105002.
[8] Í. Lacerda Fernandes, D. Pereira Barbosa, S. Botelho de Oliveira, V. Antônio da Silva, M. Henrique Sousa, M. Montero-Muñoz, J.A.H. Coaquira, Synthesis and characterization of the MNP@SiO2@TiO2 nanocomposite showing strong photocatalytic activity against methylene blue dye, Appl. Surf. Sci. 580 (2022) 152195, https://doi.org/10.1016/j.apsusc.2021.152195.
[9] L. Zhang, C. Xiao, Z. Li, J. Guo, G. Du, X. Cheng, Y. Jia, Degradation of methyl orange using persulfate activated by magnetic CuS/Fe3O4 catalyst: catalytic performance and mechanisms, Appl. Surf. Sci. 618 (2023) 156595, https://doi.org/10.1016/j.apsusc.2023.156595.
[10] A. Gil, F.C.C. Assis, S. Albeniz, S.A. Korili, Removal of dyes from wastewaters by adsorption on pillared clays, Chem. Eng. J. 168 (2011) 1032–1040, https://doi.org/10.1016/j.cej.2011.01.078.
[11] N. Al-Bastaki, Removal of methyl orange dye and Na2SO4 salt from synthetic waste water using reverse osmosis, Chem. Eng. Process. Process Intensif. 43 (2004) 1561–1567, https://doi.org/10.1016/j.cep.2004.03.001.
[12] R. Gonzalez-Olmos, U. Roland, H. Toufar, F.-D. Kopinke, A. Georgi, Fe-zeolites as catalysts for chemical oxidation of MTBE in water with H2O2, Appl. Catal. B Environ. 89 (2009) 356–364, https://doi.org/10.1016/j.apcatb.2008.12.014.
[13] A.K. Haritash, C.P. Kaushik, Biodegradation aspects of polycyclic aromatic hydrocarbons (PAHs): a review, J. Hazard. Mater. 169 (2009) 1–15, https://doi.org/10.1016/j.jhazmat.2009.03.137.
[14] U.T.D. Thuy, N.Q. Liem, C.M.A. Parlett, G.M. Lalev, K. Wilson, Synthesis of CuS and CuS/ZnS core/shell nanocrystals for photocatalytic degradation of dyes under visible light, Catal. Commun. 44 (2014) 62–67, https://doi.org/10.1016/j.catcom.2013.07.030.
[15] Y. Zhang, S. Liu, W. Lu, L. Wang, J. Tian, X. Sun, In situ green synthesis of au nanostructures on graphene oxide and their application for catalytic reduction of 4-nitrophenol, Catal, Sci. Technol. 1 (2011) 1142–1144, https://doi.org/10.1039/C1CY00205H.
[16] Y. Xu, X. Shi, R. Hua, R. Zhang, Y. Yao, B. Zhao, T. Liu, J. Zheng, G. Lu, Remarkably catalytic activity in reduction of 4-nitrophenol and methylene blue by Fe3O4@COF supported noble metal nanoparticles, Appl. Catal. B Environ. 260 (2020) 118142, https://doi.org/10.1016/j.apcatb.2019.118142.
[17] C. Peng, Z. Kuai, X. Li, S. Lian, D. Jiang, J. Tang, L. Li, R. Wu, A. Wu, S. Chen, Facile synthesis of ag nanoparticles/Ti3C2Tx/polyacrylamide composite hydrogel as efficient catalyst for methylene blue and 4-nitrophenol reduction, Mater. Des. 210 (2021) 110061, https://doi.org/10.1016/j.matdes.2021.110061.
[18] X.-Q. Zhang, R.-F. Shen, X.-J. Guo, X. Yan, Y. Chen, J.-T. Hu, W. Lang, Bimetallic ag-cu nanoparticles anchored on polypropylene (PP) nonwoven fabrics: superb catalytic efficiency and stability in 4-nitrophenol reduction, Chem. Eng. J. 408 (2021) 128018, https://doi.org/10.1016/j.cej.2020.128018.
[19] J. Guo, J. Zhang, M. Zhu, D. Ju, H. Xu, B. Cao, High-performance gas sensor based on ZnO nanowires functionalized by au nanoparticles, Sensors Actuators B Chem. 199 (2014) 339–345, https://doi.org/10.1016/j.snb.2014.04.010.
[20] M. Arumugam, R. Koutavarapu, K.-K. Seralathan, S. Praserthdam, P. Praserthdam, Noble metals (Pd, ag, Pt, and au) doped bismuth oxybromide photocatalysts for improved visible light-driven catalytic activity for the degradation of phenol, Chemosphere 324 (2023) 138368, https://doi.org/10.1016/j.chemosphere.2023.138368.
[21] X. Huang, D. Lin, P. Duan, H. Chen, Y. Zhao, W. Yang, Q. Pan, X. Tian, Space-confined growth of nanoscale metal-organic frameworks/Pd in hollow mesoporous silica for highly efficient catalytic reduction of 4-nitrophenol, J. Colloid Interface Sci. 629 (2023) 55–64, https://doi.org/10.1016/j.jcis.2022.09.075.
[22] N. Basavegowda, K. Mishra, Y.R. Lee, Trimetallic FeAgPt alloy as a nanocatalyst for the reduction of 4-nitroaniline and decolorization of rhodamine B: a comparative study, J. Alloys Compd. 701 (2017) 456–464, https://doi.org/10.1016/j.jallcom.2017.01.122.
[23] K. Saha, S.S. Agasti, C. Kim, X. Li, V.M. Rotello, Gold Nanoparticles in chemical and biological sensing, Chem. Rev. 112 (2012) 2739–2779, https://doi.org/10.1021/cr2001178.
[24] M. Kim, Y.W. Lee, D. Kim, S. Lee, S.-R. Ryoo, D.-H. Min, S.B. Lee, S.W. Han, Reshaping nanocrystals for tunable Plasmonic substrates, ACS Appl. Mater. Interfaces 4 (2012) 5038–5043, https://doi.org/10.1021/am3015058.
[25] H. Jang, S.-R. Ryoo, K. Kostarelos, S.W. Han, D.-H. Min, The effective nuclear delivery of doxorubicin from dextran-coated gold nanoparticles larger than nuclear pores, Biomaterials 34 (2013) 3503–3510, https://doi.org/10.1016/j.biomaterials.2013.01.076.
[26] J.W. Hong, S.-U. Lee, Y.W. Lee, S.W. Han, Hexoctahedral au nanocrystals with high-index facets and their optical and surface-enhanced Raman scattering properties, J. Am. Chem. Soc. 134 (2012) 4565–4568, https://doi.org/10.1021/ja300598u.
[27] A. Sahoo, S.K. Tripathy, N. Dehury, S. Patra, A porous trimetallic au@Pd@Ru nanoparticle system: synthesis, characterisation and efficient dye degradation and removal, J. Mater. Chem. A 3 (2015) 19376–19383, https://doi.org/10.1039/c5ta03959b.
[28] H. Zhang, H. Wang, J. Cao, Y. Ni, Hierarchical cu-Ni-Pt dendrites: two-step electrodeposition and highly catalytic performances, J. Alloys Compd. 698 (2017) 654–661, https://doi.org/10.1016/j.jallcom.2016.12.212.
[29] X. Li, C. Zhang, C. Du, Z. Zhuang, F. Zheng, P. Li, Z. Zhang, W. Chen, Trimetallic au@PdPt core-shell nanoparticles with ultrathin PdPt skin as highly stable electrocatalysts for the oxygen reduction reaction in acid solution, Sci. China Chem. 62 (2019) 378–384, https://doi.org/10.1007/s11426-018-9375-2.
[30] Z. Gong, T. Ma, F. Liang, Syntheses of magnetic blackberry-like Ni@cu@Pd nanoparticles for efficient catalytic reduction of organic pollutants, J. Alloys Compd. 873 (2021) 159802, https://doi.org/10.1016/j.jallcom.2021.159802.
[31] H. Zhang, N. Toshima, Preparation of novel au/Pt/ag trimetallic nanoparticles and their high catalytic activity for aerobic glucose oxidation, Appl. Catal. A Gen. 400 (2011) 9–13, https://doi.org/10.1016/j.apcata.2011.03.015.
[32] H. Zhang, L. Lu, Y. Cao, S. Du, Z. Cheng, S. Zhang, Fabrication of catalytically active au/Pt/Pd trimetallic nanoparticles by rapid injection of NaBH4, Mater. Res. Bull. 49 (2014) 393–398, https://doi.org/10.1016/j.materresbull.2013.09.025.
[33] G.T. Fu, B.Y. Xia, R.G. Ma, Y. Chen, Y.W. Tang, J.M. Lee, Trimetallic PtAgCu@PtCu core@shell concave nanooctahedrons with enhanced activity for formic acid oxidation reaction, Nano Energy 12 (2015) 824–832, https://doi.org/10.1016/j.nanoen.2015.01.041.
[34] A.A. Meshram, S.M. Sontakke, Catalytic reduction of organic pollutants using novel Ni-Ce-Zr trimetallic metal organic framework, Mater. Today Proc. (2022), https://doi.org/10.1016/j.matpr.2022.05.500.
[35] T.T.D. Nguyen, D. Van Dao, N. Thi Thu Ha, T. Van Tran, D.S. Kim, J.W. Yoon, N. N. Ha, I.H. Lee, Y.T. Yu, Superhigh sensing response and selectivity for hydrogen gas using PdPt@ZnO core-shell nanoparticles: unique effect of alloyed ingredient from experimental and theoretical investigations, Sensors Actuators B Chem. 354 (2022) 131083, https://doi.org/10.1016/j.snb.2021.131083.
[36] J. Zhu, X. Zhang, Z. Qin, L. Zhang, Y. Ye, M. Cao, L. Gao, T. Jiao, Preparation of PdNPs doped chitosan-based composite hydrogels as highly efficient catalysts for reduction of 4-nitrophenol, colloids surfaces a physicochem, Eng. Asp. 611 (2021) 125889, https://doi.org/10.1016/j.colsurfa.2020.125889.
[37] T. Baran, Biosynthesis of highly retrievable magnetic palladium Nanoparticles stabilized on bio-composite for production of various Biaryl compounds and catalytic reduction of 4-Nitrophenol, Catal. Lett. 149 (2019) 1721–1729, https://doi.org/10.1007/s10562-019-02753-3.
[38] W. Yang, Q. Zhang, C. Peng, E. Wu, S. Chen, Y. Ma, J. Hou, Y. He, B. Zhang, L. Deng, Au@PdAg core-shell nanotubes as advanced electrocatalysts for methanol electrooxidation in alkaline media, RSC Adv. 9 (2019) 931–939, https://doi.org/10.1039/C8RA08781D.
[39] E. Wu, Q. Zhang, A. Xie, W. Yang, C. Peng, J. Hou, Y. He, B. Zhang, L. Deng, Synthesis of hollow echinus-like au@PdAgNSs decorated reduced graphene oxide as an excellent electrocatalyst for enhanced ethanol electrooxidation, J. Alloys Compd. 789 (2019) 174–182, https://doi.org/10.1016/j.jallcom.2019.03.086.
[40] K. Thongthai, P. Pakawanit, N. Chanlek, J.-H. Kim, S. Ananta, L. Srisombat, Ag/au/Pt trimetallic nanoparticles with defects: preparation, characterization, and electrocatalytic activity in methanol oxidation, Nanotechnology 28 (2017) 375602, https://doi.org/10.1088/1361-6528/aa846b.
[41] V. Vongsavat, B.M. Vittur, W.W. Bryan, J.-H. Kim, T.R. Lee, Ultrasmall hollow gold–silver nanoshells with extinctions strongly red-shifted to the near-infrared, ACS Appl. Mater. Interfaces 3 (2011) 3616–3624, https://doi.org/10.1021/am2008322.
[42] E.R. Carmona, N. Benito, T. Plaza, G. Recio-Sánchez, Green synthesis of silver nanoparticles by using leaf extracts from the endemic Buddleja globosa hope, Green Chem. Lett. Rev. 10 (2017) 250–256, https://doi.org/10.1080/17518253.2017.1360400.
[43] A.M.R. Simões, N.A.M. Saraiva, C.V.R. de Moura, E.M. de Moura, J.C.S. Costa, Trimetallic nanotubes: a bifunctional substrate for the catalytic and spectroscopic study using surface-enhanced Raman spectroscopy, Vib. Spectrosc. 115 (2021), https://doi.org/10.1016/j.vibspec.2021.103274.
[44] Y. Bao, K. Chen, AgCl/ag/g-C3N4 hybrid composites: preparation, visible light-driven photocatalytic activity and mechanism, Nano-Micro Lett. 8 (2016) 182–192, https://doi.org/10.1007/s40820-015-0076-y.
[45] H.A. Elazab, M.A. Sadek, T.T. El-Idreesy, Microwave-assisted synthesis of palladium nanoparticles supported on copper oxide in aqueous medium as an efficient catalyst for Suzuki cross-coupling reaction, Adsorpt. Sci. Technol. 36 (2018) 1352–1365, https://doi.org/10.1177/0263617418771777.
[46] K. Leus, P. Concepcion, M. Vandichel, M. Meledina, A. Grirrane, D. Esquivel, S. Turner, D. Poelman, M. Waroquier, V. Van Speybroeck, G. Van Tendeloo, H. García, P. Van Der Voort, Correction: au@UiO-66: a base free oxidation catalyst, RSC Adv. 5 (2015) 26726, https://doi.org/10.1039/C5RA90022K.
[47] Z.G. Asmare, B.A. Aragaw, M. Atlabachew, T.A. Wubieneh, Kaolin-supported silver Nanoparticles as an effective catalyst for the removal of methylene blue dye from

aqueous solutions, ACS Omega 8 (2023) 480–491, https://doi.org/10.1021/acsomega.2c05265.
[48] S. Sabahat, Y. Nazish, A. Akhtar, A. Shahid, Nanoengineering of mono (au, ag) and bimetallic (ag-au) alloy nanoparticles for dye degradation and toxicity assessment, Spectrochim. Acta - part a Mol, Biomol. Spectrosc. 321 (2024), https://doi.org/10.1016/j.saa.2024.124705.
[49] M.J. Ahemad, T.D. Le, D.S. Kim, Y.T. Yu, Bimetallic AgAualloy@ZnO core-shell nanoparticles for ultra-high detection of ethanol: potential impact of alloy composition on sensing performance, Sensors Actuators B Chem. 359 (2022), https://doi.org/10.1016/j.snb.2022.131595.
[50] H.B. Ahmed, H.E. Emam, Seeded growth core-shell (ag–au–Pd) ternary nanostructure at room temperature for potential water treatment, Polym. Test. 89 (2020) 106720, https://doi.org/10.1016/j.polymertesting.2020.106720.
[51] K. Suwannarat, K. Thongthai, S. Ananta, L. Srisombat, Synthesis of hollow trimetallic ag/au/Pd nanoparticles for reduction of 4-nitrophenol, Colloids Surf. A Physicochem. Eng. Asp. 540 (2018) 73–80, https://doi.org/10.1016/j.colsurfa.2017.12.046.
[52] F. Ahmadpoor, M. Nasrollahzadeh, M. Mohammad, Self-assembled lignosulfonate-inorganic hybrid nanoflowers and their application in catalytic reduction of methylene blue and 4-nitrophenol, Sep. Purif. Technol. 272 (2021) 118864, https://doi.org/10.1016/j.seppur.2021.118864.
[53] B. Akilandaeaswari, K. Muthu, One-pot green synthesis of au-ag bimetallic nanoparticles from Lawsonia inermis seed extract and its catalytic reduction of environmental polluted methyl orange and 4-nitrophenol, J. Taiwan Inst. Chem. Eng. 127 (2021) 292–301, https://doi.org/10.1016/j.jtice.2021.07.019.
[54] K. Muthu, S. Priya, Green synthesis, characterization, and catalytic activity of silver nanoparticles using Cassia auriculata flower extract separated fraction, Spectrochim, Acta Part A Mol. Biomol. Spectrosc. 179 (2017) 66–72, https://doi.org/10.1016/j.saa.2017.02.024.
[55] Y. Sha, I. Mathew, Q. Cui, M. Clay, F. Gao, X. Jackie, Z. Gu, Chemosphere Rapid degradation of azo dye methyl orange using hollow cobalt nanoparticles 144 (2016) 1530–1535, https://doi.org/10.1016/j.chemosphere.2015.10.040.
[56] E.E. Altuner, R.N. El Houda Tiri, A. Aygun, F. Gulbagca, F. Sen, A. Iranbakhsh, F. Karimi, Y. Vasseghian, E.N. Dragoi, Hydrogen production and photocatalytic activities from NaBH4 using trimetallic biogenic PdPtCo nanoparticles: development of machine learning model, Chem. Eng. Res. Des. 184 (2022) 180–190, https://doi.org/10.1016/j.cherd.2022.05.021.
[57] T. Nanoparticles, Facile One-Pot Biogenic Synthesis of cu-co-Ni Dye Degradation, 2020.
[58] K.K. Haldar, S. Tanwar, R. Biswas, T. Sen, J. Lahtinen, Noble copper-silver-gold trimetallic nanobowls: an efficient catalyst, J. Colloid Interface Sci. 556 (2019) 140–146, https://doi.org/10.1016/j.jcis.2019.08.047.
[59] Y.-J.L, E.S.Y. Yan-Yan Shen, Yue Sun, Lin-Nan Zhou, Synthesis of ultrathin PtPdBi nanowire and its enhanced catalytic activity towards p-nitrophenol reduction †, J. Mater. Chem. A 2 (2014) 2977–2984, https://doi.org/10.1039/c3ta14502f.
[60] N.R. Jana, Z.L. Wang, T. Pal, Redox catalytic properties of palladium Nanoparticles: surfactant and Electron donor−acceptor effects, Langmuir 16 (2000) 2457–2463, https://doi.org/10.1021/la990507r.
[61] H.M.A. Sharif, A. Mahmood, H.Y. Cheng, R. Djellabi, J. Ali, W.L. Jiang, S. Sen Wang, M.R. Haider, N. Mahmood, A.J. Wang, Fe3O4 Nanoparticles coated with EDTA and ag Nanoparticles for the catalytic reduction of organic dyes from wastewater, ACS Appl. Nano Mater. 2 (2019) 5310–5319, https://doi.org/10.1021/acsanm.9b01250.
[62] K.D. Daware, R.N. Shinde, C.V. Khedkar, S.I. Patil, A.K. Pandey, M. Ashokkumar, S. W. Gosavi, Enhanced catalytic activity of platinum decorated silica nanocrystals in rapid reduction of organic dyes, Chem. Phys. Impact 5 (2022) 100109, https://doi.org/10.1016/j.chphi.2022.100109.
[63] Q. He, D. Yu, T. Ma, J. Bao, J. Wang, J. Zhang, J. Cheng, W. Fan, J. Li, One step reduction of coral-like palladium–gold–copper trimetallic alloy nanoparticles (Pd–au–cu NPs) and its investigation as photothermal-enhanced Fenton catalytic degradation of organic dye pollutants, Mater. Chem. Phys. 332 (2025) 130296, https://doi.org/10.1016/j.matchemphys.2024.130296.
[64] A. Kumar Maddheshiya, N. Yadav, S. Yadav, P. Singh Yadav, T. Prasad Yadav, Facial synthesis of the trimetallic au-Pt-Pd nanofluids and performance for methylene blue degradation, Mater. Lett. 349 (2023) 134735, https://doi.org/10.1016/j.matlet.2023.134735.
[65] A. Chalgin, F. Shi, F. Li, Q. Xiang, W. Chen, C. Song, P. Tao, W. Shang, T. Deng, J. Wu, Ternary Pt-Pd-ag alloy nanoflowers for oxygen reduction reaction electrocatalysis, CrystEngComm 19 (2017) 6964–6971, https://doi.org/10.1039/c7ce01721a.



Sonalika Agarwal is currently working as a Research Scientist at Hiroshima University, Japan, with extensive experience in materials science. She received her Ph.D. in 2012 from the University of Rajasthan, India. Following this, she served as an Assistant Professor at KIET Group of Institutions, India (2012–2016). In 2017, she was honored with the prestigious DST Women Scientist Award and conducted research at Malaviya National Institute of Technology (MNIT) Jaipur, India, until 2021. In 2020, she received the prestigious BRICS Young scientist Award in the field of material science. She then held postdoctoral positions at Jeonbuk National University, South Korea (2021–2022), and served as a Visiting Research Scientist at Universitat Rovira i Virgili, Spain (2023). Her research focuses on the design and development of functional nanomaterials, including 1D, 2D, and 3D nanostructures; metal oxides (MOSs); transition metal dichalcogenides (TMDs); core-shell structures; noble metal and alloy nanoparticles; and polymer nanocomposites. These hybrid materials are applied in gas sensing, optoelectronics, catalytic reduction, membrane separation, and energy-related applications.



Dong-Seog Kim is currently a Ph.D. candidate at the Division of Advanced Materials Engineering, Jeonbuk National University, South Korea. He obtained his master's degree (MS) in 2022 from Jeonbuk National University. Gas sensors with core-shell nanoparticles are the focus of his study.



Lakshmana Reddy Nagappagari obtained his Ph.D. in 2018 from Yogi Vemana University, India. Then he worked as research associate in Institute of Nano Science and Technology, Mohali, India, followed by Postdoctoral researcher in Kyungpook National University, South Korea (2018-2020). Later he served as Brain Korea BK21 researcher in Jeonbuk National University, South Korea (2021-2022). Currently he is working as senior postdoctoral research in KU Leuven University, Belgium. Dr. Reddy has wide research experience in synthesizing several nanostructured catalytic materials including nanoparticles, quantum dots, TiO_2 nanotubes, nanorods, nanobelts, composites of metal oxides, 2D C_3N_4 nanosheets based composites, core-shell structures, hematite based photoanodes, Single Atom Catalysts, MOFs in the application of solar light photoelectrocatalytic water splitting for H2 generation and also environmental remediation applications.



Yeon-Tae Yu is a professor in the Division of Advanced Materials Engineering at Jeonbuk National University, South Korea. He received his B.S. and M.S. degrees from Jeonbuk National University in 1988 and 1988, respectively, and received Doctoral degree in 1993 from Tohoku University, Japan. From 1993 to 2003, he was a Senior Researcher at Korea Institute of Geoscience and Mineral Resources (KIGAM). In 2004, he moved to Division of Advanced Materials Engineering of Jeonbuk National University as Assistant Professor. His current research interests are synthesis of core-shell structure composite nanoparticles and their applications for photocatalysts, gas sensors and fuel cells.